Bioactive Materials 26 (2023) 323–336

Contents lists available at ScienceDirect

Bioactive Materials

journal homepage: www.keaipublishing.com/en/journals/bioactive-materials

Exosome/metformin-loaded self-healing conductive hydrogel rescues microvascular dysfunction and promotes chronic diabetic wound healing by inhibiting mitochondrial fission

Yue Zhang [a,1], Meng Li [b,c,1], Yunchuan Wang [a,1], Fei Han [a], Kuo Shen [a], Liang Luo [a], Yan Li [a], Yanhui Jia [a], Jian Zhang [a], Weixia Cai [a], Kejia Wang [a], Ming Zhao [a], Jing Wang [a], Xiaowen Gao [a], Chenyang Tian [a], Baolin Guo [b,c,**], Dahai Hu [a,*]

[a] Department of Burns and Cutaneous Surgery, Xijing Hospital, Fourth Military Medical University, 127 Changle West Road, Xi'an, Shaanxi, 710032, China
[b] State Key Laboratory for Mechanical Behavior of Materials, And Frontier Institute of Science and Technology, Xi'an Jiaotong University, Xi'an, 710049, China
[c] Key Laboratory of Shaanxi Province for Craniofacial Precision Medicine Research, College of Stomatology, Xi'an Jiaotong University, Xi'an, 710049, China

ARTICLE INFO

Keywords:
Dual-loaded hydrogels
Adipose-derived mesenchymal stem cell exosomes
Metformin
Angiogenesis
Mitochondrial fission
Chronic diabetic wound
Wound healing

ABSTRACT

Chronic diabetic wounds remain a globally recognized clinical challenge. They occur due to high concentrations of reactive oxygen species and vascular function disorders. A promising strategy for diabetic wound healing is the delivery of exosomes, comprising bioactive dressings. Metformin activates the vascular endothelial growth factor pathway, thereby improving angiogenesis in hyperglycemic states. However, multifunctional hydrogels loaded with drugs and bioactive substances synergistically promote wound repair has been rarely reported, and the mechanism of their combinatorial effect of exosome and metformin in wound healing remains unclear. Here, we engineered dual-loaded hydrogels possessing tissue adhesive, antioxidant, self-healing and electrical conductivity properties, wherein 4-armed SH-PEG cross-links with Ag^{+}, which minimizes damage to the loaded goods and investigated their mechanism of promotion effect for wound repair. Multiwalled carbon nanotubes exhibiting good conductivity were also incorporated into the hydrogels to generate hydrogen bonds with the thiol group, creating a stable three-dimensional structure for exosome and metformin loading. The diabetic wound model of the present study suggests that the PEG/Ag/CNT-M + E hydrogel promotes wound healing by triggering cell proliferation and angiogenesis and relieving peritraumatic inflammation and vascular injury. The mechanism of the dual-loaded hydrogel involves reducing the level of reactive oxygen species by interfering with mitochondrial fission, thereby protecting F-actin homeostasis and alleviating microvascular dysfunction. Hence, we propose a drug–bioactive substance combination therapy and provide a potential mechanism for developing vascular function-associated strategies for treating chronic diabetic wounds.

1. Introduction

By 2019, 463 million cases (20–79 years) of diabetes, a complex metabolic disorder, had been detected worldwide, and the number is expected to reach 578 million cases by 2030 [1]. Chronic wounds are one of the most serious diabetic complications, eventually leading to amputations in ~25% patients, of whom at least 68% die within 5 years [2,3]. The primary characteristic of these wounds is increased levels of reactive oxygen species (ROS) due to persistent hyperglycemia, inducing excessive oxidative stress and impaired antioxidant capacity [4] and causing microvascular injury, angiogenesis inhibition, and prolonged inflammatory response [5]. Reportedly, mitochondrial dynamics, particularly mitochondrial fission, have been strongly associated with hyperglycemia-induced ROS formation and vascular damage [6–9],

Peer review under responsibility of KeAi Communications Co., Ltd.
* Corresponding author.
** Corresponding author. State Key Laboratory for Mechanical Behavior of Materials, and Frontier Institute of Science and Technology, Xi'an Jiaotong University, Xi'an, 710049, China.
E-mail addresses: baoling@mail.xjtu.edu.cn (B. Guo), hudhai@fmmu.edu.cn (D. Hu).
[1] These authors share first authorship.

https://doi.org/10.1016/j.bioactmat.2023.01.020
Received 7 November 2022; Received in revised form 8 January 2023; Accepted 27 January 2023

disrupting cell integrity and barrier function and delaying neovascularization [10,11].

Adipose-derived stem cells (ADSCs) are vital in cutaneous regeneration, angiogenesis, inflammation, and extracellular cellular matrix (ECM) remodeling [12–14]. Exosomes, a key ADSCs secretory product (Fig. 1A), have been identified as the primary contributor to the therapeutic effect of the latter [15]. Exosomes have nanoscale dimensions and immune tolerability comparable to stem cells. Further, exosomes can be utilized to transfer proteins, mRNAs, miRNAs, and other small molecular substances into recipient cells to activate regeneration-related signaling pathways and ameliorate oxidative stress-associated skin injury by reducing ROS production [16], thereby decreasing DNA damage, mitochondrial changes, histological injuries, and inflammation [17–20]. Direct injection of adipose-derived mesenchymal stem cell exosomes

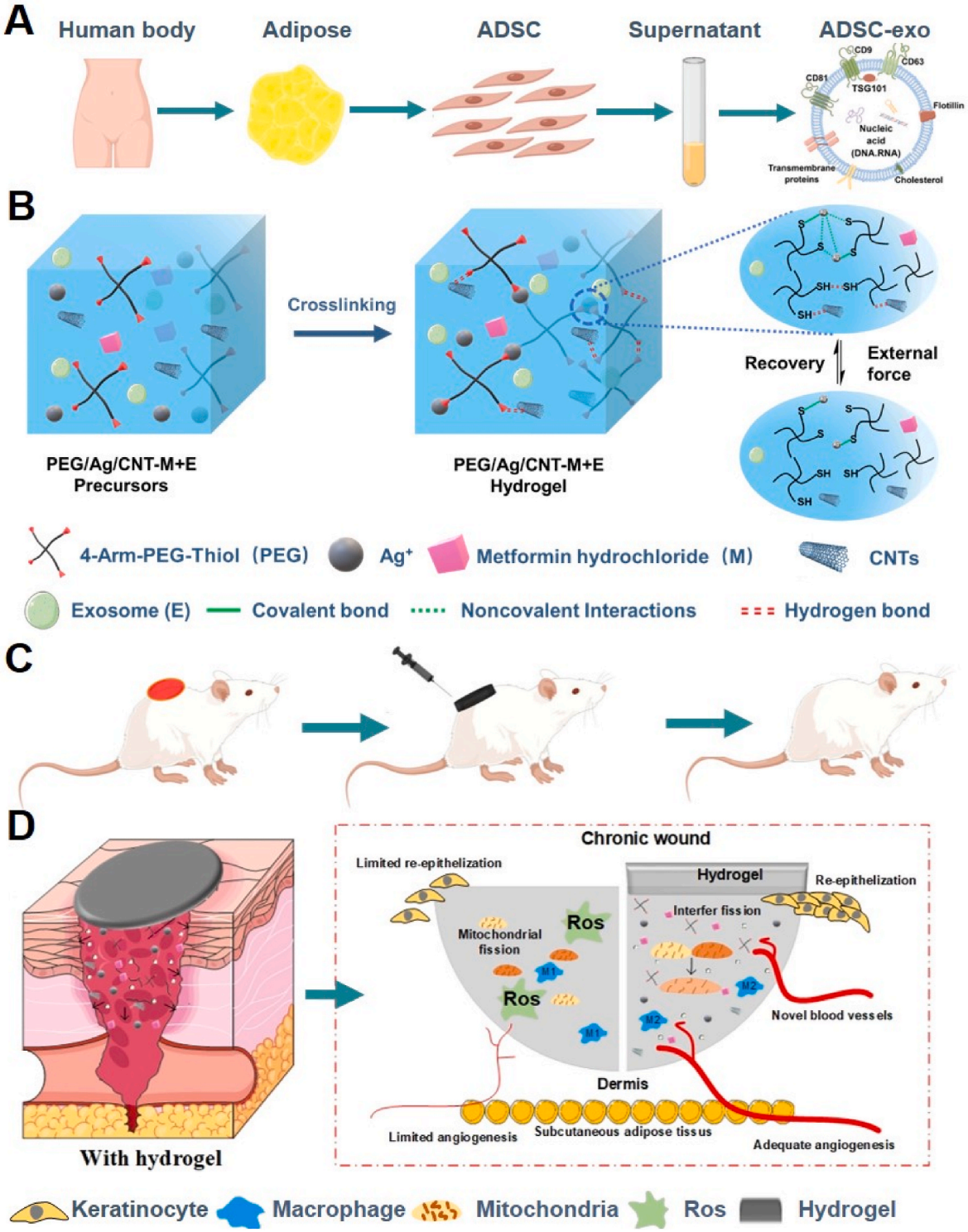

Fig. 1. Schematic overview of the preparation and application of the PEG/Ag/CNT-M + E hydrogel for chronic wound. (A) Isolation of ADSCs and ADSC-Exos. (B) The synthesis diagram of the PEG/Ag/CNT-M + E hydrogel. (C, D) The PEG/Ag/CNT-M + E hydrogel was applied on the diabetic mouse, wherein it promoted wound healing by triggering cell proliferation and angiogenesis, reduced the level of ROS by interfering with mitochondrial fission.

(ADSC-Exos) is the most common method of exosome administration; however, their rapid clearance and short half-life *in vivo* hinder their clinical application [21], especially as diabetic wound healing requires a long time and repeated injections.

Metformin, a frequently used drug for diabetes, plays an important role in microvascular protection in high glucose environment. It reduces hyperglycemia-induced endothelial cell damage via mitochondrial autophagy [22]. Furthermore, it inhibits proinflammatory cytokine and adhesion molecule expressions via AMPK pathway activation and NF-κB signaling activity inhibition in vascular endothelial cells [23]. Besides, hyperglycemia is an important diabetic complication and glucose control is crucial for determining the complexity and variability of the physiological environment of diabetic wounds. Metformin increases the susceptibility of peripheral cells to insulin [24,25], thus showing a good effect in glucose control. Reportedly, metformin-loaded reactive release systems accelerate the healing of diabetic foot wounds [26]. The drug–bioactive agent combination synergistically promotes wound healing [27,28] but it remains unclarified whether the combinatorial effect of metformin and exosome is additive or synergistic in chronic diabetic wound healing.

Hydrogels are three-dimensional (3D) porous polymeric networks exhibiting good hydrophilicity and biocompatibility, similar to ECM, facilitating wound healing by optimizing the biological and molecular events involved in the wound healing cascade [29–31]. They are an ideal choice for the wound surface and can be used as carriers to supplement the wound area with drugs and bioactive substances [32–34]. However, differences in crosslinking of biomaterials influence their resultant porosity, in turn affecting the loading and releasing behaviors of the drugs and bioactive substances and reducing their therapeutic effect [35]. Most importantly, chronic diabetic wound pathogenesis is complex and the underlying mechanism of hydrogel-induced wound healing remains unelucidated with direct targets still unidentified. Research in this field may facilitate the development of effective treatments for healing diabetic wounds.

Here, we designed a novel self-healing conductive hydrogel by crosslinking four-armed SH-PEG with Ag^+ and coordinating Ag–S to produce a dynamic PEG hydrogel. The conductive active material of hydroxyl-modified multiwalled carbon nanotubes (CNTs) forms hydrogen bonds with thiol, finally yielding a stable 3D structure. Metformin was selected as the model drug and ADSCs-Exos as the bioactive substance. The highly interconnected porous network formed by the coordination and crosslinking method mobilizes and releases metformin and exosomes, thus improving the utilization and reducing damage to the loaded drugs. The slow degradation and release of exosomes can overcome the disadvantage of rapid clearance inherent to direct exosome injection. The efficacy of this dual-loaded hydrogel was investigated for healing chronic diabetic wounds and their underlying mechanisms were elucidated (Fig. 1C and D). We characterized the physicochemical properties of the hydrogels, evaluated their repair effect, and explored their mechanisms with regard to oxidative stress response, vascular function, and mitochondrial dynamics.

2. Results and discussion

2.1. Preparation and characterization of the PEG/Ag/CNT-M + E hydrogel

2.1.1. Engineering of the PEG/Ag/CNT-M + E hydrogel

To address the multiple needs of chronic diabetic wound healing, a self-healing, tissue adhesive, antioxidant, provascular hydrogel loaded with 4-Arm-PEG-Thiol, Ag^+, exosomes, CNTs, and metformin hydrochloride was designed herein. The synthesis diagram of the hydrogel is presented in Fig. 1B. The main network of the hydrogel was created using the Ag–S coordination between 4-Arm-PEG-Thiol and Ag^+. Simultaneous rupture and recombination interactions among Ag^+ under external forces endowed the hydrogels with good injectability and self-healing ability. Hydrogen bonding between the sulfhydryl groups in 4-Arm-PEG-Thiol and hydroxyl group on CNTs further enhanced the mechanical strength, self-healing properties, and bioelectrical signal transmission of the PEG/Ag/CNT-M + E hydrogel. The injectable, self-healing hydrogels can adapt to wounds of different shapes and effectively prolong the service time of the wound dressing. Finally, we loaded the hydrogel with metformin and exosomes to improve the wound microenvironment and promote the vascular function of the hydrogels. Overall, the injectable, self-healing PEG/Ag/CNT-M + E hydrogel equipped with sustained metformin and exosomes release demonstrated great potential for treating chronic diabetic wounds.

2.1.2. Characterization of the PEG/Ag-series hydrogels

2.1.2.1. Morphology of the PEG/Ag-series hydrogels. The scanning electron microscopy images of the PEG/Ag-series hydrogels are depicted in Fig. 2A. The PEG-Ag hydrogel exhibited a uniform macroporous structure, indicating good crosslinking between 4-Arm-PEG-Thiol and Ag^+ via Ag–S coordination and simultaneous interactions. The internal pore size of the hydrogel slightly decreased after introducing CNTs, which may be attributable to the hydrogen bonding between the hydroxyl group of CNTs and the thiol group of 4-Arm-PEG-Thiol, further increasing the internal crosslinking of the PEG/Ag/CNT hydrogel. Moreover, compared with the PEG/Ag/CNT hydrogel, the internal structure of the PEG/Ag/CNT and PEG/Ag/CNT-M + E hydrogels did not exhibit significant changes, indicating that introducing metformin and exosomes did not affect the internal structure of the hydrogels and their uniform dispersal. Hence, the PEG/Ag-series hydrogels exhibit a uniform macroporous structure with the potential to facilitate wound healing by absorbing wound exudate.

2.1.2.2. Self-healing and injectable properties of the PEG/Ag/CNT-M + E hydrogel. External wound dressings, which are usually exposed, can be easily damaged by external forces, whereas the use of self-healing hydrogel wound dressings, administered internally, offers a substantially extended service life. Thus, the self-healing performance of the PEG/Ag/CNT-M + E hydrogel was evaluated using rheological tests. Strain amplitude sweep test revealed that at the maximum critical strain point (774%), G′ (storage modulus) was equal to G″ (loss modulus) of the hydrogel, indicating that the hydrogel was between the solid and fluid states. Moreover, the hydrogel structure completely degraded after undergoing maximum critical strain (strain >774%). Subsequently, a continuous strain cycle from 1% to 1000% (>1000%) was applied to assess the rheological self-healing behavior of the hydrogel. On increasing the strain from 1% to 1000%, the structure of the hydrogel completely degraded, with G″>G′. When the strain returned to 1%, the G′ and G″ of the hydrogel returned to their initial values (G′>G″), demonstrating restoration of the hydrogel structure via self-healing (Fig. 2B). The above process could be repeated numerous times, indicating the rapid, stable, and highly efficient self-healing capacity of the hydrogel. Therefore, the results of the rheological tests confirmed the self-healing properties of the hydrogel, which are attributable to the reversible simultaneous interactions between Ag+and rich hydrogen bonding in the hydrogels.

The excellent self-healing and injectable properties will impart great benefit in using the hydrogel for wound dressings, especially for wounds with different shape. Hydrogel wound dressings can be injected into different wounds, particularly deeper chronic wounds, where they can adopt different shapes and contribute to wound healing via their self-healing properties. The excellent injectable properties of the PEG/Ag/CNT-M + E hydrogels were confirmed using a macroscopic photograph (Fig. 2C) and video (Video S1).

Supplementary data related to this article can be found at https://doi.org/10.1016/j.bioactmat.2023.01.020.

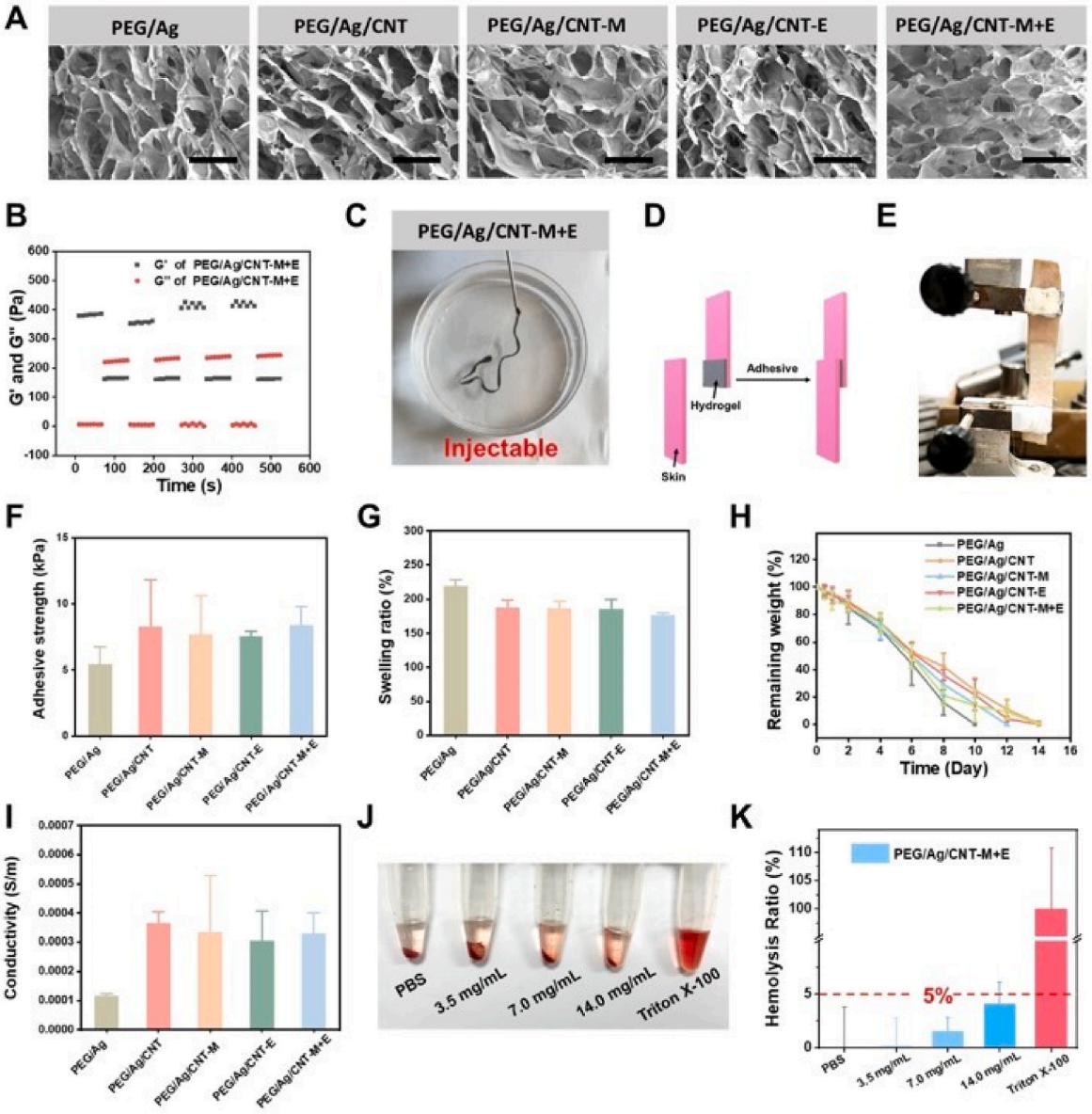

Fig. 2. Characterization of the PEG/Ag-series hydrogels. (A) Morphology of all the hydrogels; scale bar: 200 μm. (B) Evaluation of the self-healing properties of hydrogels using rheology. (C) Demonstration of the injectability of all the hydrogels. (D) and (E) Evaluation of the tissue adhesion properties of all the hydrogels. Schematic diagram of the evaluation method of hydrogel tissue adhesion: lap-shear test. (F) Demonstration and results of the tissue adhesion properties of all the hydrogels. (G) Equilibrium swelling ratio of all the hydrogels in phosphate-buffered saline (PBS). (H) *In vitro* degradation properties of all the hydrogels in PBS. (I) Conductive properties of all the hydrogels. (J) Demonstration of hemocompatibility of all the hydrogels. (K) Hemolytic ratio of all the hydrogels.

2.1.2.3. Tissue adhesion properties of the PEG/Ag-series hydrogels. The optimized tissue adhesive ability of hydrogel maintained its binding to the target wound, ensuring its effectiveness. Lap-shear test was employed to evaluate the tissue adhesive properties of the PEG/Ag-series hydrogels (Fig. 2D and E). The adhesion strength between the PEG/Ag hydrogel and skin was ~5 kPa (Fig. 2F), attributable to the hydrophilicity of PEG, covalent crosslinking and chain entanglement between the hydrogel and extracellular proteins in the tissue during *in situ* gelation, and hydrogen bonding with tissues. Introducing CNTs further increased the tissue adhesion of the PEG/Ag/CNTs hydrogel to 7–8 kPa ($P < 0.05$), probably by increasing the mechanical strength of the hydrogel and facilitating more hydrogen bonding. However, metformin and exosome addition induced no change in the hydrogel structure, as the tissue adhesion of the PEG/Ag/CNT-M, PEG/Ag/CNT-E, and PEG/Ag/CNT-M + E hydrogels were also 8 kPa. Overall, the PEG/Ag-series hydrogels exhibited higher tissue adhesion strength than fibrin glue (~5 kPa), which met the need for adhesion to the wound surface [36].

2.1.2.4. Swelling and degradation properties of the PEG/Ag-series hydrogels. Chronic diabetic wounds are often accompanied by infection and excessive wound exudate, which can be absorbed by hydrogels owing to their good swelling ability. This ability also keeps the wound environment moist, thereby facilitating wound repair [37] Thus, phosphate-buffered saline (PBS) with a pH of 7.4 was used to simulate the wound exudate environment and assess the swelling performance of the PEG/Ag-series hydrogels (Fig. 2G). The PEG/Ag hydrogel exhibited an equilibrium swelling ratio of ~220%, which increased to ~180% after introducing CNTs into PEG/Ag/CNT, PEG/Ag/CNT-M, PEG/Ag/CNT-E, and PEG/Ag/CNT-M + E, as it increased the crosslinking density of the hydrogels.

After the hydrogel swelling was equilibrated, its degradation *in vitro*

in PBS (pH = 7.4) was evaluated. The PEG/Ag hydrogel completely degraded on the 10th day. The degradation of the PEG/Ag/CNT, PEG/Ag/CNT-M, PEG/Ag/CNT-E, and PEG/Ag/CNT-M + E hydrogels were completed on the 12–14th day owing to their stronger hydrogen bonding and crosslinking owing to CNTs (Fig. 2H). Hence, the swelling ratios of the PEG/Ag-series hydrogels indicated longer stability in the wound exudate environment, which can meet the needs of appropriate wound dressings.

2.1.2.5. Conductive properties of the PEG/Ag-series hydrogels. The human skin exhibits conductive properties, with its electrical conductivity varying from 2.6 to 1×10^{-4} mS/cm. After skin damage, an endogenous induction electric field of 40–200 mV/mm is triggered in the wound area to initiate healing [38]. Adding electroactive materials to skin transmit bioelectrical signals and promote skin cell proliferation, migration, and adhesion, thereby accelerating healing, particularly in chronic wounds [39–41]. Hence, combining modern biomaterials with electroactive substances is ideal for developing novel dressings. Multiwalled CNTs have been reported to be promising for skin tissue engineering owing to their excellent electrical conductivity, biocompatibility, antimicrobial activity, high drug loading capacities, high mechanical strength, and large surface areas [42,43]. Here we incorporated multiwalled CNTs into a hydrogel to synthesize a hydrogel dressing for treating chronic diabetic wounds. The PEG/Ag hydrogel exhibits a conductivity of 1.15×10^{-4} S/m owing to the ionic conductivity of silver ions after the addition of CNTs. The conductivities of PEG/Ag/CNT, PEG/Ag/CNT-M, PEG/Ag/CNT-E, and PEG/Ag/CNT-M + E hydrogels increased to the range of 3.04–3.65 $\times 10^{-4}$ S/m, indicating that CNTs further enhanced the conductivity of the hydrogels, facilitating electrical signal transmission from living biological tissue and promoting wound healing (Fig. 2I).

2.1.2.6. Hemocompatibility of the PEG/Ag/CNT-M + E hydrogel. When the body contact with biomaterials that does not have proper hemocompatibility will led to undesired responses, such as the rupturing of red blood cells, the formation of thrombosis and inflammation at the wound site [44]. This phenomenon can disturb the normal wound healing process. Hence, hemocompatibility is critical for effective wound dressing. The study has reported that a hemolysis ratio of <5% represents good hemocompatibility. [45–47]' *In vitro* hemolytic activity tests were employed to evaluate the hemocompatibility of the PEG/Ag/CNT-M + E hydrogel. The color of the supernatant following the hydrolysis of the hydrogels with a polymer concentration gradient of 3.5–14 mg/mL was similar to that of PBS (Fig. 2J), indicating that the PEG/Ag/CNT-M + E hydrogel demonstrated good hemocompatibility. The supernatants were subsequently collected for quantitative analysis (Fig. 2K) and it was found that the hemolysis ratios at different concentrations of the hydrogels were <5%, exhibiting good hemocompatibility. Overall, the PEG/Ag/CNT-M + E hydrogel showed good hemocompatibility as wound dressing.

2.1.2.7. Release behavior of metformin and Ag^+ ions from hydrogels. The sustained release of drugs and bioactive substances further enhance their efficacy in wound healing. Generally speaking, more than 10 days' drug release property *in vivo* and vitro environment could exhibited the promising application of hydrogels in drug sustained release carriers [48]. The release properties of metformin in the PEG/Ag/CNT-M and PEG/Ag/CNT-M + E hydrogel were tested. Fig. S1 showed that metformin release from the PEG/Ag/CNT-M hydrogel has no statistical differences from the PEG/Ag/CNT-M + E hydrogel. In the PEG/Ag/CNT-M + E hydrogel, the drug release was 37% ± 11.25% on day 2, continuing to increase to 90.2% ± 8.23% on day 12. For diabetic wounds, metformin could increase the susceptibility of peripheral cells to insulin; hence, the release character of metformin from the PEG/Ag/CNT-M + E hydrogel is advantageous for treating diabetic wounds. Besides, Ag^+ is a well-known antibacterial agent that has commonly been used to promote wound healing. The cumulative release of Ag^+ from the PEG/Ag/CNT-M + E hydrogel was 40.2% ± 8.56% on day 2, continuing to increase to 95.66% ± 5.73% on day 12, with no statistical differences compared with the other PEG/Ag-series hydrogels (Fig. S2), thereby confirming the sustained release characteristics of drugs of the hydrogels.

2.2. Characterization of ADSC-Exos

The process of ADSC-Exos collection is shown in Fig. 3A. ADSCs were extracted from human adipose tissues and cultured *in vitro*. The cells displayed a remarkable fibroblast-like morphology (Fig. 3B). Osteogenic and adipogenic inductions showed calcium deposition and lipid droplet presence via Alizarin Red S staining and Oil Red O staining, respectively (Fig. 3B). Immunofluorescence assay revealed that these cells overexpressed laminin, an ECM marker, and SOX2, a pluripotent marker (Fig. 3C). Flow cytometry demonstrated that the surface markers of ADSCs, including CD44 (FITC 97.5%), CD105 (FITC 99.1%), and CD90 (FITC 98.4%), were highly positive, but negative for hematopoietic stem cell surface markers CD34 (FITC 1.6%), CD31 (FITC 1.8%), and CD11b (FITC 2.0%) (Fig. 3D). The ADSC-Exos were extracted using differential centrifugation, and their size ranged between 50 and 150 nm, as revealed by high-sensitivity flow cytometry for nanoparticle analysis (Fig. 3E). The typical double-layer cup-shaped membranous structures of ADSC-Exos were observed under electron microscopy (Fig. 3F). Western blot confirmed the expression of the exosomal surface markers CD9, CD63, and TSG101 (Fig. 3G). These data confirmed a successful extraction of ADSCs and their exosomes. In addition, laser confocal microscopy revealed that the exosomes were encapsulated by the PEG/Ag/CNT-M + E hydrogel (Fig. 3H, Video S2). The exosome release profiles (Fig. 3I) showed that the bioactive exosomes underwent sustained released for 12 days, during which > 80% of them underwent unimpeded release from the PEG/Ag/CNT-M + E hydrogel, showing no significant difference from their release from the PEG/Ag/CNT-E hydrogel. Moreover, after 10 days of PKH26-labeled PEG/Ag/CNT-M + E hydrogel treatment, immunofluorescence staining of the mouse skin wound tissue could still detected the immunofluorescent signal of the exosomes (Fig. 3J).

Supplementary data related to this article can be found at https://doi.org/10.1016/j.bioactmat.2023.01.020.

2.3. PEG/Ag/CNT-M + E hydrogel improves wound healing in a diabetic mouse model

We tested the healing-promoting effect of the PEG/Ag-series hydrogels in a diabetic mouse wound model. The blood glucose levels of all the blood samples collected from the tail vein of the mouse were >16.7 mmol/L. A round, full-thickness skin injury (1-cm diameter) was established on the back of the mouse. Tegaderm dressing was applied in the control group, with PEG conductive hydrogel representing the PEG/Ag/CNT group, exo-loaded conductive hydrogel representing the PEG/Ag/CNT-E group, metformin-loaded conductive hydrogel representing the PEG/Ag/CNT-M group, and exo and metformin coloaded conductive hydrogel representing the PEG/Ag/CNT-M + E group. The samples were harvested at the corresponding time points as shown in the schematic diagram in Fig. 4A. The wound area gradually reduced over time after injury (Fig. 4B). Following 3 days of treatment, the wound length of the PEG/Ag/CNT-M + E hydrogel group was significantly smaller than that of the other groups (Fig. 4F, $p < 0.01$). The PEG/Ag/CNT-M + E group exhibited the fastest wound healing rate at all the time points, and the wound virtually closed on the 10th day following treatment (Fig. 4G, $p < 0.001$); hence, the addition of exosomes and metformin to the hydrogels significantly promoted the healing of diabetic mice wounds. Both PEG/Ag/CNT-M and PEG/Ag/CNT-E hydrogels exhibited enhanced wound healing, but the efficacy has no significant difference

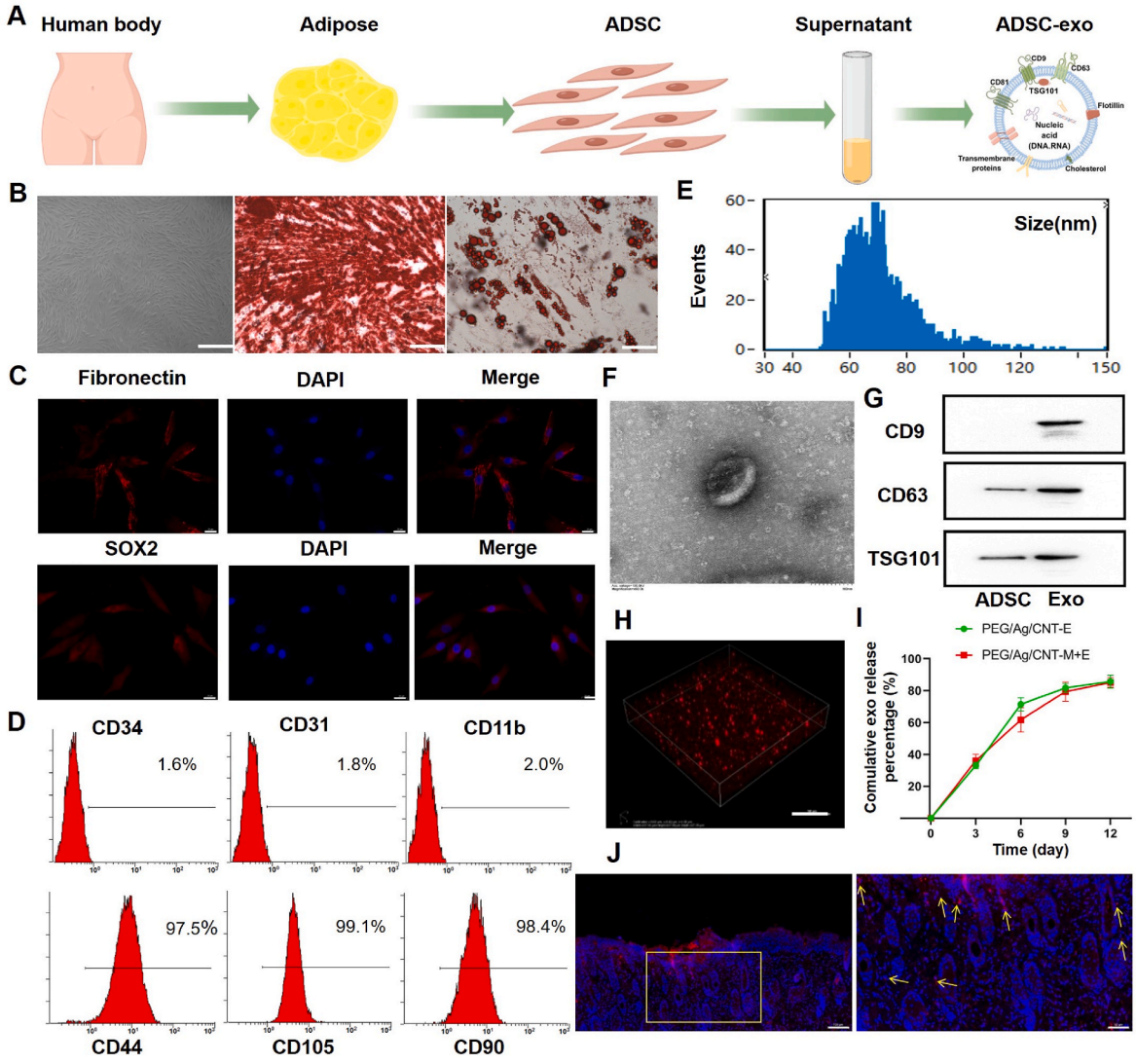

Fig. 3. Characterization of ADSCs and ADSC-Exos. (A) Isolation of ADSCs and ADSC-Exos. (B) Optical morphology of ADSCs under light field microscope; scale = 400 μm. Osteogenic and adipogenic differentiations were examined using Alizarin Red S and Oil Red O staining, respectively; scale bar = 50 μm. (C) Immunofluorescent staining of ADSCs; > 90% cells were positivity for the ECM marker, fibronectin, and the pluripotency marker, Sox2; scale bar: 20 μm. (D) Identification of ADSCs using flow cytometry. The results showed positive expressions of CD44, CD105, and CD90; negative expressions of CD34, CD31, and CD11b. (E) Nanoparticle tracking analysis of exosomes. (F) ADSC-Exos morphology analysis using electron microscopy; scale bar = 100 nm. (G) Western blotting of exosome markers CD9, CD63, and TSG101. (H) Confocal 3D of exosomes in the PEG/Ag/CNT-M + E hydrogel. (I) ADSC-Exos release curves in the PEG/Ag/CNT-E and PEG/Ag/CNT-M + E hydrogel. (J) Immunofluorescence staining of mouse skin wound tissue treated with PKH26-labeled PEG/Ag/CNT-M + E hydrogel. Data are showed as mean ± SD (n = 3/group, *p < 0.05, **p < 0.01, ***p < 0.001).

between the two groups.

The wound tissues were further subjected to hematoxylin and eosin (H&E) and Masson staining and the wound diameter, granulation, and epithelialization of the wound bed 14 days after the injury were histologically assessed. H&E staining revealed good growth of granulation tissues, with the PEG/Ag/CNT-M + E group showing the shortest wound length and complete epithelization, indicating a good healing outcome (Fig. 4C). The arrangement and distribution of collagen are important criterion for assessing wound healing. Appropriate collagen deposition favors wound repair, whereas excessive and disorganized collagen deposition causes scar hypertrophy and deters wound repair. Masson staining was performed to observe collagen distribution in the wounds of the different treatment groups (Fig. 4D). The collagenous fibers were neatly organized in the PEG/Ag/CNT-M + E group, indicating the potential to reduce scar formation. This group also demonstrated well-formed and -arranged hair follicle structures. The observations of both H&E and Masson staining suggest that the PEG/Ag/CNT-M + E hydrogel is ideal for promoting diabetic wound healing. Vascular function is essential for wound healing as it expands the vascular network, further affecting cell metabolism, oxygen transportation, and nutrient absorption. We used scanning electron microscopy to observe the morphological microvascular changes in each sample (Fig. 4E). Compared with the wounds of nondiabetic mice, diabetic wound exhibited vascular edema, lumen stenosis, hyperplasia, and basement membrane (BM) thickness, accompanied by reduced number of intercellular tight junctions (TJ). These characteristics were reversed by the PEG/Ag/CNT-M + E hydrogel. The PEG/Ag/CNT-M + E group showed a more complete and continuous BM, and the number of TJ between the cells were increased.

Ki67 is an important marker for assessing cellular proliferation. Immunofluorescence staining of skin tissue revealed the strongest immunofluorescent Ki67 signal in the PEG/Ag/CNT-M + E group (Fig. 5A), which was statistically significant (Fig. 5C, $p < 0.001$). This indicated that the PEG/Ag/CNT-M + E hydrogel promoted wound

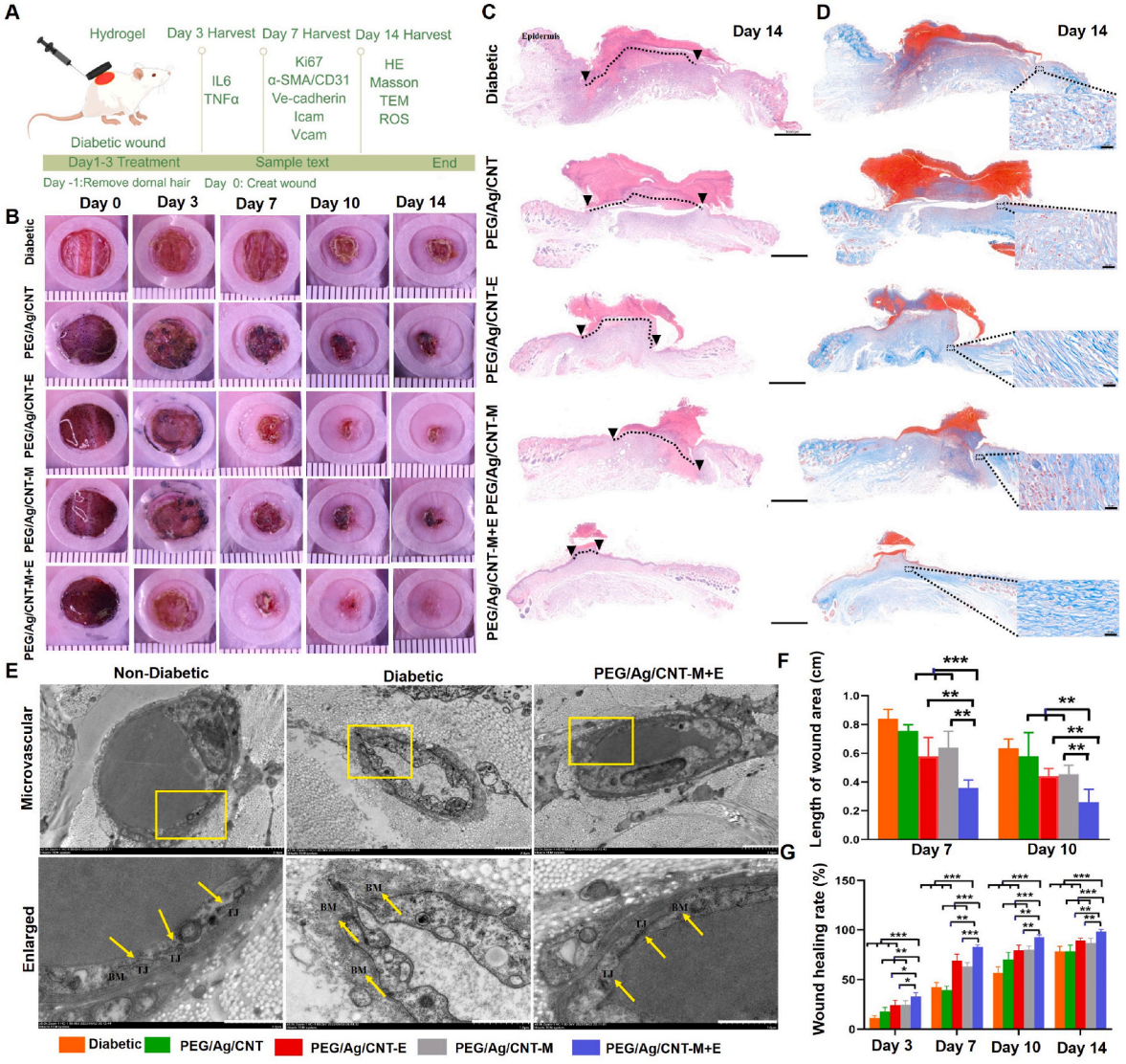

Fig. 4. Effects of the PEG/Ag-series hydrogels on wound healing in a diabetic mouse model. (A) Schematic diagram of the experimental processes. (B) Digital photographs of the wound areas dressed with Tegaderm or PEG/Ag-series hydrogels on days 0, 3, 7, 10, and 14; scale bar = 1 cm. (C) Representative hematoxylin and eosin results of the wound tissue in each group on day 14; scale bar = 1 mm. (D) Representative Masson staining of the wound tissue in each group on day 14; scale bar = 20 μm. (E) Representative electron microscopy images of microvascular changes in the basement membrane of skin wound tissue in each group. (F)Analysis of the wound length on day 7 and 10 in each group. (G)Analysis of the wound closure rate in each group at each timepoint. The data are shown as the mean ± SD (n = 5/group, *p < 0.05, **p < 0.01, ***p < 0.001).

healing by enhancing cell proliferation. Blood vessels provide nutrition and oxygen to the skin and are critical for wound healing. Hence, treatments for chronic wounds involve strategies to improve endothelial dysfunction, reduce inflammatory responses, and promote wound revascularization [49,50] CD31 is a marker of wound neovascularization, and aSMA is a marker of mature vessels [51-55] aSMA/CD31 dual fluorescence assay revealed the highest density and quantity of blood vessels with large lumens and intact structures in the PEG/Ag/CNT-M + E group 7 days after injury compared with the other groups (Fig. 5B,D,5E). Hence, these findings indicate that exosome and metformin addition engenders a synergistic effect on angiogenesis and vessel maturation.

The disruption of endothelial integrity and loss of barrier function due to inflammatory responses delay wound healing. Ve-cadherin is an important adhesion molecule of endothelial cells and is vital in maintaining vascular integrity and stability [56,57] Our immunofluorescence results revealed reduced Ve-cadherin expression in diabetic wounds and a higher expression in the groups treated with PEG/Ag/CNT-M + E hydrogel (Fig. 5F and I). Diabetic wounds exhibit significantly upregulated expressions of cell adhesion molecules Icam and Vcam, which are essential for driving vascular inflammatory responses. Compared with the other groups, the groups treated with PEG/Ag/CNT-M + E hydrogel showed significantly decreased Icam and Vcam levels (Fig. 5G, H, 5J, 5K $p < 0.001$). Together, these data reveal the beneficial effects of exosomes and metformin on maintaining vascular integrity and barrier function in diabetic wounds, which are conducive to reducing vascular inflammation, promoting cell proliferation and angiogenesis, and accelerating wound healing.

Reportedly, the inflammatory response peaks on the 3rd day following injury, gradually decreasing thereafter, after which the next stage of wound healing begins [58,59]. Although the inflammation stage of chronic wounds is hard to control, strategies for shortening the prolonged inflammatory response have proven effective in accelerating the healing time [60–63]. IL-6 and TNF-α are important proinflammatory cytokines that inhibit chronic wound healing [64–66]. On the 3rd day after injury, IL-6 and TNF-α expressions of each group were evaluated

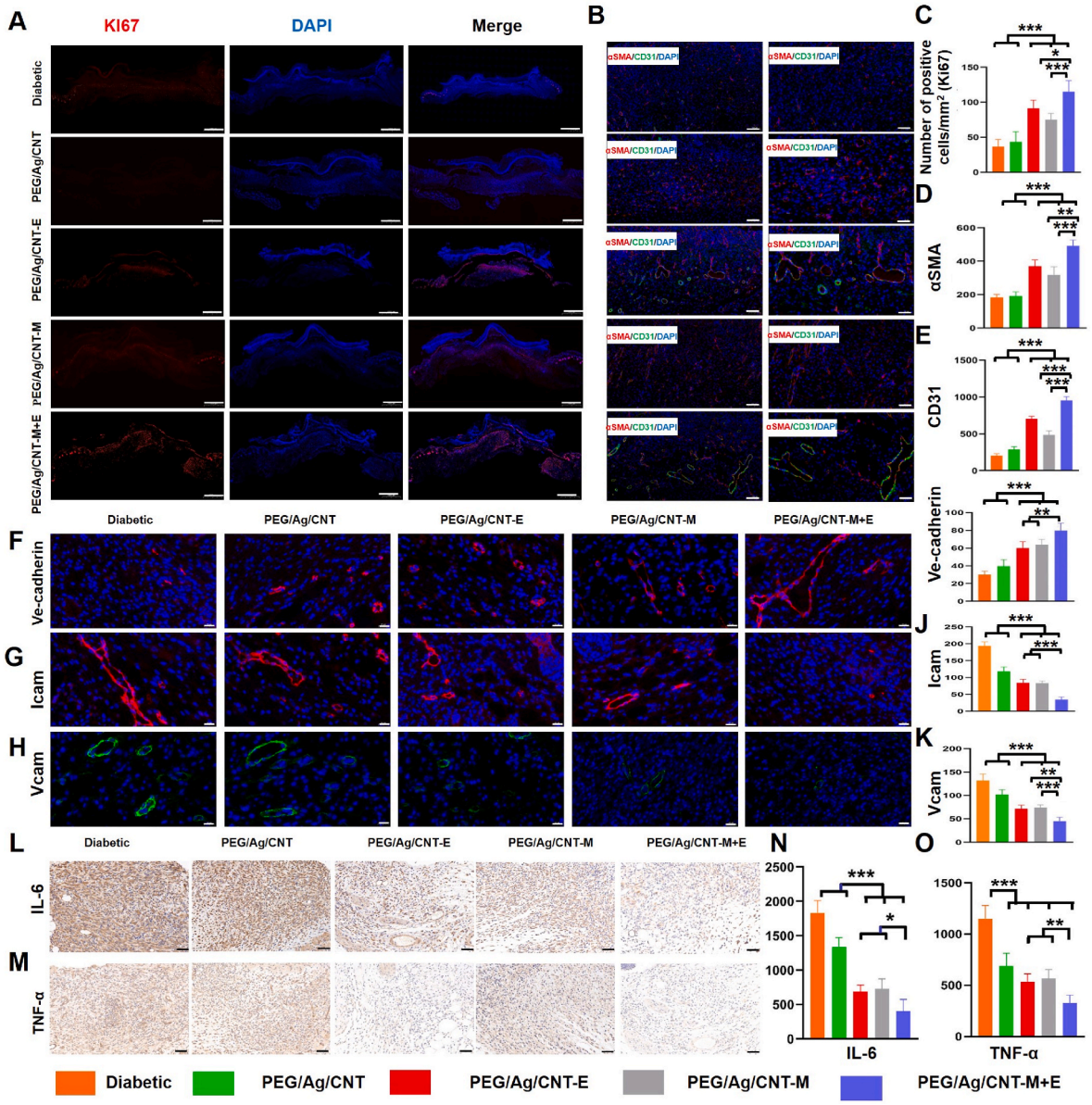

Fig. 5. Impact of the PEG/Ag-series hydrogels on wound healing in a diabetic mouse model. (A) Representative photographs of Ki67 immunofluorescence staining of skin wound tissue on day 7 after injury; scale = 1 cm. (B) Representative images of αSMA and CD31 immunofluorescence staining of skin wound tissue on day 7 after injury; scale = 100 μm in left; scale = 50 μm in right. (C) Statistical data of relative Ki67 expression of the different groups. Statistical data of the relative expression of (D) αSMA and (E) CD31. (F–H) Representative images of Ve-cadherin, Icam, and Vcam immunofluorescence staining of skin wound tissue on day 7 after injury; scale = 20 μm. Statistical data of the relative expression of (I) Ve-cadherin, (J) Icam, and (K) Vcam.(L) Representative photographs of immunohistochemistry staining of IL-6 and (M) TNF-α of skin wound tissue on day 3 after injury (scale = 50 μm). (N) Statistical data of the relative expression of IL-6 and (O) TNF-α. (n = 5/group, *p < 0.05, **p < 0.01, ***p < 0.001).

via immunohistochemical staining. As shown in Fig. 4L and M, the levels of IL-6 and TNF-α were much lower in the PEG/Ag/CNT-M + E group than in the other groups (Fig. 5N,O), confirming that metformin and exosomes synergistically suppress the inflammatory response in diabetic wounds, thereby improving the microenvironment for wound healing.

2.4. Biocompatibility of the PEG/Ag/CNT-M + E hydrogel

After observing the ideal healing-promoting effect of this dual-loaded hydrogel in animals, its *in vitro* effects on cellular behavior were investigated. We explored the underlying mechanism of exosomes and metformin in human umbilical vein endothelial cells (HUVECs) [67–69]. To assay the biological effects of exosomes *in vitro*, we first confirmed PKH26-labeled exosomes could be absorbed by HUVECs (Fig. S3). Then the viability of HUVECs in Dulbecco's modified eagle medium (DMEM; control), high glucose (33 mM), and high glucose + PEG/Ag-series hydrogels were determined after 3 days of culturing. The staining results revealed only a few nonviable cells in each groups (Fig. S4), and there were no difference in the number of viable cells among all the groups (Fig. S5), thereby confirming the good cyto-compatibility of endothelial cells with the PEG/Ag-series hydrogels. Cell proliferative, migratory, and tube-forming capabilities of the hydrogels were further assayed. Ki67 immunofluorescence assay revealed the highest number of Ki67-positive cells in the PEG/Ag/CNT-M + E group (Fig. 6A), consistent with the animal experiment results. Besides, the proportion of Ki67-expressing cells was more in the PEG/Ag/CNT-M or PEG/Ag/CNT-E hydrogel group than in the control group (Fig. 6B; $p < 0.001$). These data confirm the synergistic effect of metformin and

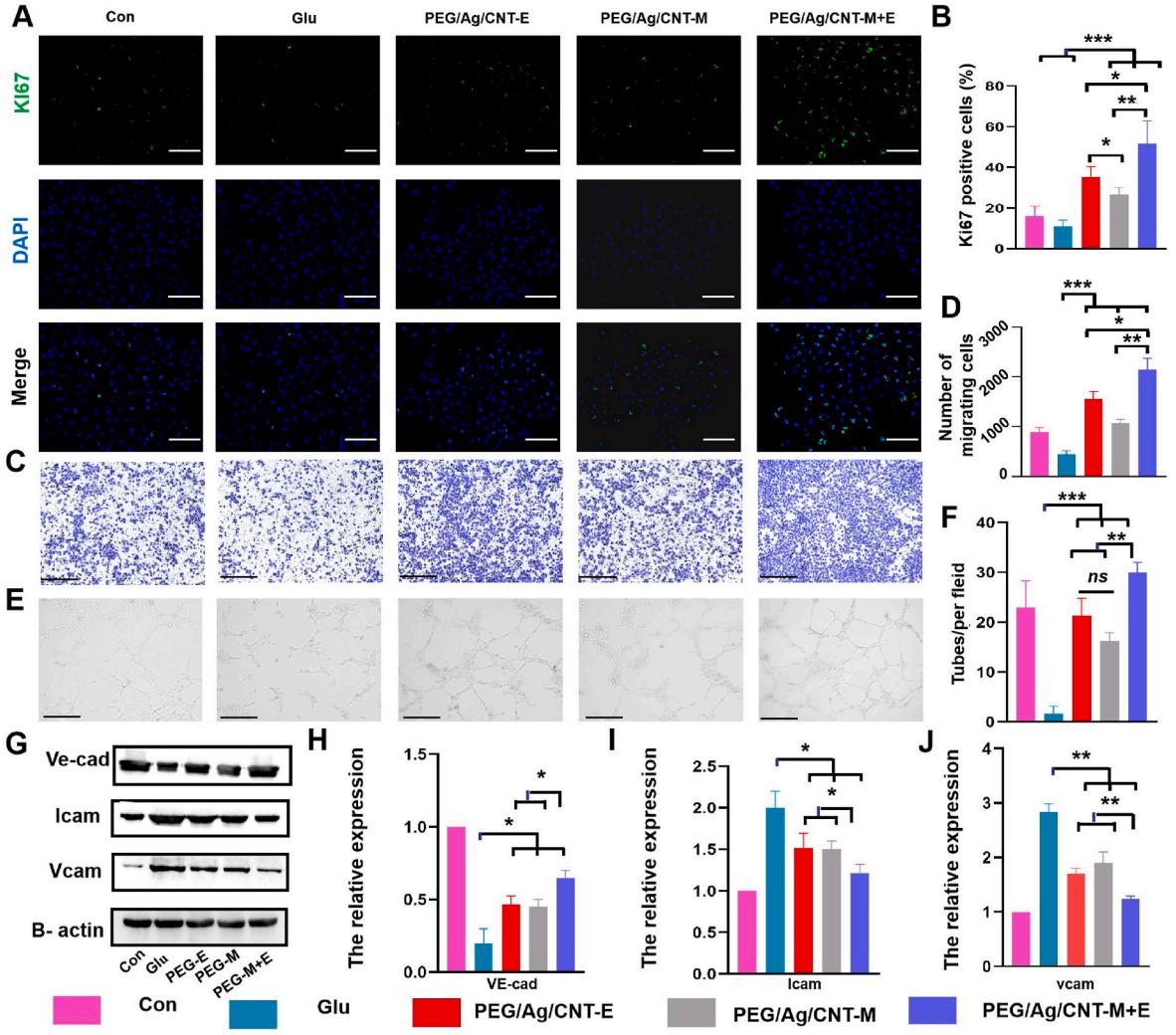

Fig. 6. Effects of the PEG/Ag-series hydrogels on HUVECs. (A) Effect of the PEG/Ag-series hydrogels on HUVECs proliferation was determined using Ki67 immunofluorescence assays; scale = 275 μm. (B) Statistical data of the relative expression of Ki67. (C) Effect of the PEG/Ag-series hydrogels on HUVECs migration was examined using Transwell assay at 8 h following cocolture; scale bar = 1 cm. (D) Quantification of the number of migrated HUVECs.(E) Angiogenesis in the different groups; scale = 650 μm. (F) Quantification of the number of tubes per field. (G–J) The Western blot results of Ve-cadherin, Icam, and Vcam expression (n = 3/group, *p < 0.05, **p < 0.01, ***p < 0.001).

exosomes on promoting HUVECs proliferation in high-glucose environments. Transwell assay results demonstrated a greater promotion of cell migration in the PEG/Ag/CNT-M + E group than other groups (Fig. 6C and D). The most pronounced tubular formation and intact tubular structures were also observed in the PEG/Ag/CNT-M + E group (Fig. 6E and F). The Western blot results were consistent with those of the animal experiments. In a high-glucose environment, Ve-cadherin expression in HUVECs decreased, whereas the expressions of Icam and Vcam increased. However, the dual-loaded hydrogel restored Ve-cadherin expression and decreased those of the inflammatory chemokines, Icam and Vcam (Fig. 6G–J). Hence, these data suggest that the PEG/Ag/CNT-M + E hydrogel exhibits stronger cytoprotection toward HUVECs and promotes cell proliferation, migration, and angiogenesis in a high-glucose environment.

2.5. *PEG/Ag/CNT-M + E hydrogel alleviates ROS production in high glucose levels*

The dual-loaded hydrogel exhibited ideal microvascular protection and healing-promoting effects both *in vivo* and *in vitro*; however, the underlying mechanism by which the hydrogel influences diabetic microangiogenesis remains largely unknown. Abnormal metabolism engendered by diabetes produces excessive ROS [70–72], consequently triggering various cellular mechanisms, including protein kinase C activation, NF-kB-mediated vascular inflammation, structural and functional vascular impairment, and alterations in vascular permeability, neovascularization, and cell proliferation [73]. Excessive ROS production is an important pathology of endothelial injury and vasculopathy in diabetic wounds (Fig. 7A) [74–76]. To verify the impact of the dual-loaded hydrogel on vascular functions via the regulation of ROS production, ROS fluorescence assay of the mouse skin tissue was performed 14 days after injury. The fluorescence in the dual-loaded hydrogel group was significantly lower than that in the untreated Diabetic group (Fig. 7B). Flow cytometry revealed that the dual-loaded hydrogel effectively inhibited ROS production in HUVECs cultured in a high-glucose media (Fig. 7C).

Mitochondrial ROS (mtROS), NADPH oxidase, and xanthine oxidase production are involved in ROS production induced by high glucose. Mitochondria produce excessive mtROS and are the primary source of cellular ROS production in the presence of high-glucose environment, inducing oxidative stress and tissue damage [77,78]. Hence, targeting mtROS production is important for improving the vascular health of diabetic wounds [79] Multiple regulatory modes, such as mitochondrial dynamics (mitochondrial fusion and fission), mitochondrial kinetics,

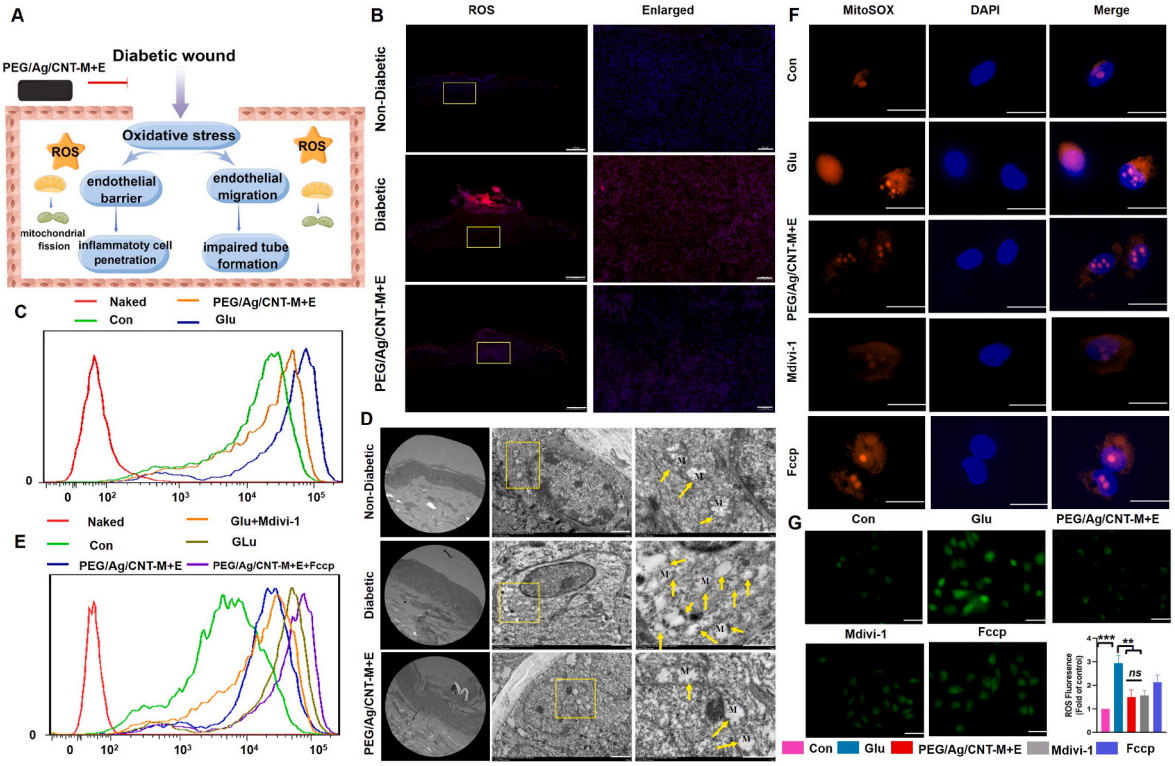

Fig. 7. PEG/Ag/CNT-M + E hydrogel reduces ROS production in a high-glucose environment, partially recovering diabetes-distorted mitochondrial morphology. (A) Schematic diagram indicating the proposed mechanisms underlying the protection against microvasculature damage provided by the dual-loaded hydrogel in a high-glucose environment. (B) Representative images of ROS expression in the mouse skin wound tissue; scale bar = 1 cm. (C) Detected expressions of ROS in HUVECs in each group using flow cytometry. (D) PEG/Ag/CNT-M + E hydrogel partially rescued diabetes-distorted mitochondrial morphology in the skin wound tissue; scale bar = 2 μm on the left, detailed scale bar = 1 μm in the middle. (E)Detected expressions of ROS in HUVECs in each group using flow cytometry. (F) HUVECs mitochondrial ROS expression in different groups.(G) HUVECs ROS expression in different groups was examined using immunofluorescence assays; scale bar = 825 μm. (H) Quantitative statistical data of HUVECs ROS in each group. (n = 3/group, *p < 0.05, **p < 0.01, ***p < 0.001).

and mitochondrial membrane potential changes, affect mtROS production. Notably, mitochondrial fission is essential for excessive mtROS production induced by high glucose.[80] Mitochondria undergo rapid fragmentation, upregulate fission-associated proteins, dynamin-related protein 1 (Drp1) and Fis1 expressions, and increase mtROS production [81] Remarkably, metformin also inhibits *Drp1*-mediated mitochondrial fission to protect adipose tissue from oxidative damage induced by high-glucose environment [82] The dual-loaded hydrogel effectively reduced ROS production in tissues and cells. However, it remains unknown whether the action mechanism of this hydrogel is associated with mitochondrial dynamic and whether it can reduce ROS production by relieving mitochondrial fission. The exact role of mitochondrial dynamics in diabetic wound healing remains to be explored. Here, we used scanning electron microscopy to observe the mitochondrial morphology of the skin wound cells (Fig. 7D). The results revealed that the mitochondria were slightly swollen and tubular cristae were reserved in nondiabetic mice wounds, whereas in the diabetic mice wound, the outer mitochondrial membrane was damaged and the mitochondrial structure had disappeared, disintegrating into numerous circular fragments of different sizes. In the PEG/Ag/CNT-M + E group, the intracellular mitochondrial morphology was partially preserved, demonstrating the protective effect of the hydrogel on mitochondrial morphology.

To assess the effects of mitochondrial fission on ROS production *in vitro*, we treated HUVECs with high glucose levels in the presence of the mitochondrial fission inhibitor, mdivi-1, and the mitochondrial fission activator, fccp. Flow cytometry and immunofluorescence staining results showed that both mdivi-1 and the PEG/Ag/CNT-M + E hydrogel reduced ROS production compared with the high glucose control, whereas fccp partially counteracted the inhibitory effect on ROS production observed in the PEG/Ag/CNT-M + E group (Fig. 7E,G). MtROS staining further confirmed (Fig. 7F) higher mtROS levels in the high-glucose environment, while mdivi-1 and PEG/Ag/CNT-M + E groups restricted mtROS production. Fccp counteracted the mtROS scavenging effect of the PEG/Ag/CNT-M + E hydrogel. The results indicate that high glucose-induced cellular ROS and mtROS production can be reversed by the PEG/Ag/CNT-M + E hydrogel, potentially by inhibiting mitochondrial fission.

2.6. *PEG/Ag/CNT-M + E hydrogel improves vascular function in high-glucose environments by inhibiting mitochondrial fission*

Mitochondrial staining was performed to detect the effect of the dual-loaded hydrogel on mitochondrial fission at the cellular level (Fig. 8A). The mitochondria in the high glucose group became smaller, punctate, and considerably shorter in length, while most of the mitochondria in the dual-loaded hydrogel and mdivi-1 groups exhibited a filamentous morphology. The results suggest that the PEG/Ag/CNT-M + E hydrogel inhibits the high glucose-induced mitochondrial fission, whereas the fission activator fccp counteracted the fission protection of the dual-loaded hydrogel. Drp1 is a key mediator and promoter of mitochondrial fission. Colocalization staining of Drp1 and mitochondria (Fig. 8B) revealed increased Drp1 expression on the mitochondrial surface in the high glucose group, while decreased expression in the PEG/Ag/CNT-M + E and mdivi-1 groups. Western blot results of mitochondrial fission- and fusion-related proteins (Fig. 8C) demonstrated that fusion proteins Mfn1 and Mfn2 were upregulated in the PEG/Ag/CNT-M + E and mdivi-1 groups, while fission proteins Drp1, Fis1, and Mff were downregulated (Fig. 8D and E). It was further confirmed that the dual-loaded hydrogel inhibited mitochondrial fission in HUVECs in a

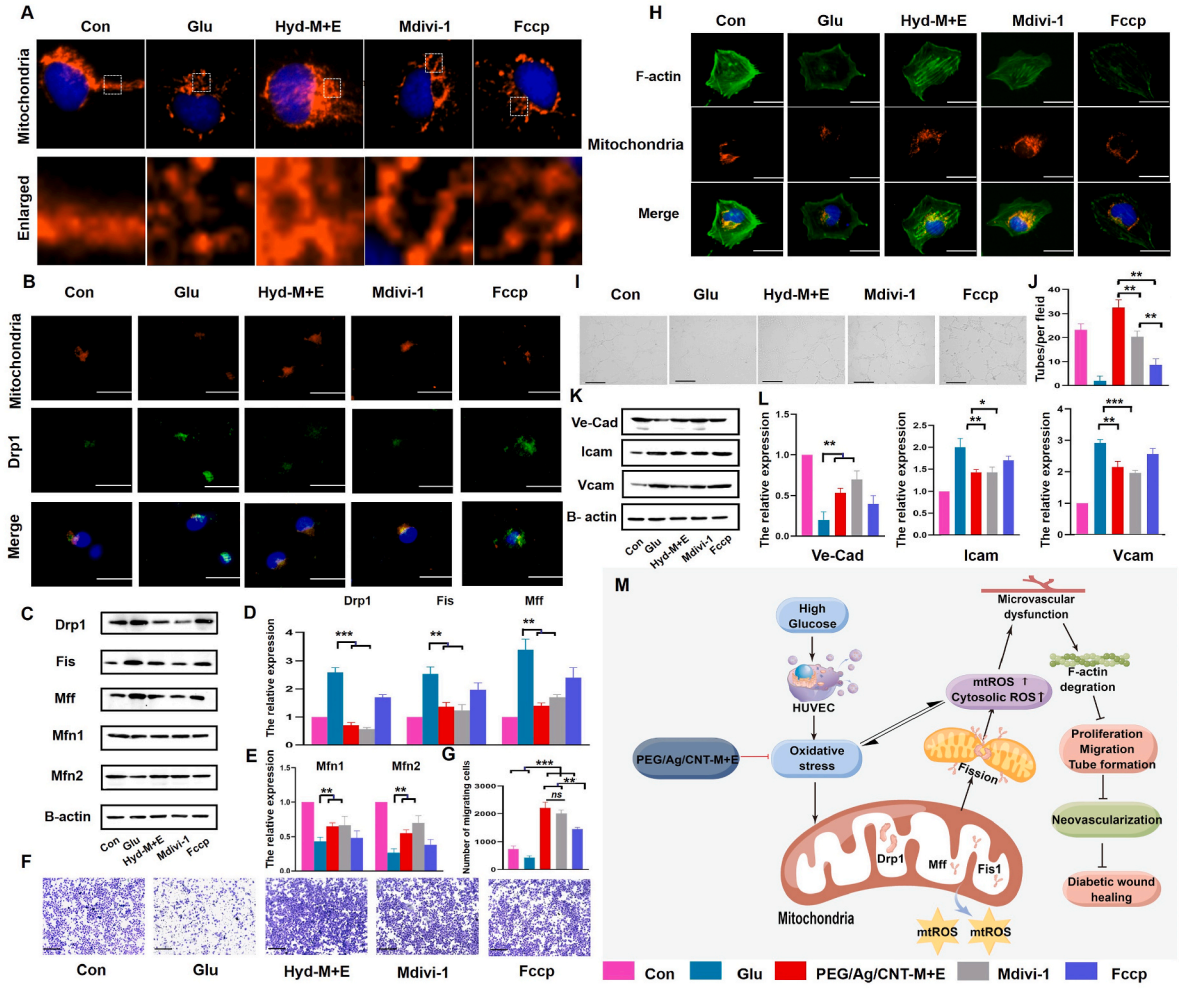

Fig. 8. PEG/Ag/CNT-M + E hydrogel reduced mitochondrial fission in a high-glucose environment and partially rescued HUVECs function by maintaining F-actin homeostasis. (A) Mitochondrion-selective MitoFluor™ staining was used to label HUVECs mitochondria and mitochondrial morphology was analyzed using fluorescence microscopy; scale bar = 12.88 μm. (B) Colocalization of Drp1 and mitochondria. (C–E) Changes in mitochondrial fission- and fusion-related protein expressions in HUVECs. (F) Effect of mitochondrial fission on HUVECs migration examined using the Transwell assay; scale bar = 1 cm. (G) Quantification of the number of migrated HUVECs. (H) Coimmunofluorescence of mitochondria and F-actin to analyze the relationship between mitochondrial fission and F-actin homeostasis; scale bar = 45.83 μm. Mitochondria fission was accompanied by F-actin dissolution. The results were reversed by the PEG/Ag/CNT-M + E hydrogel and mdivi1. (I) Effect of mitochondria fission and angiogenesis in different groups; scale bar = 650 μm (J) Quantification of the number of tubes per field. (K, L) Ve-cadherin, Icam, and Vcam expressions in HUVECs of each group. (M) Schematic diagram showing the proposed mechanisms of the dual-loaded hydrogel protection against mitochondrial fission and partially rescued HUVECs function in a high-glucose environment (n = 3/group, *p < 0.05, **p < 0.01, ***p < 0.001).

high-glucose environment.

Finally, we assessed the relationship between mitochondrial fission and the function of partially rescued HUVECs. Transwell assay results revealed that HUVECs mobility was impaired in a high-glucose environment and that the dual-loaded hydrogel and mdivi-1 groups partially restored this process (Fig. 8F and G). F-actin is a crucial stress fiber for endothelial cell mobilization, and impaired vascular endothelial cell migration in a high-glucose environment has been strongly associated with F-actin homeostasis dysregulation [83–85]. The relationship between F-actin and mitochondrial fission has been previously studied [86]. F-actin decomposes into G-actin on mitochondrial fission initiation and reassembles into F-actin on the outer mitochondrial membrane, indicating its indispensable nature in mitochondrial fission. Excessive fission consumes large amounts of F-actin, ultimately causing F-actin homeostasis dysregulation and impaired migration [87–89]. Here, we co-staining mitochondria and F-actin in HUVECs of different groups as shown in Fig. 8H; in the PEG/Ag/CNT-M + E and mdivi-1 groups, mitochondrial fission was reduced and the filamentous F-actin structure was preserved. In the high glucose and fccp groups, mitochondrial fragmentation was accompanied by F-actin dissolution and disappearance. In addition, the *in vitro* proangiogenetic effects in the PEG/Ag/CNT-M + E hydrogel and mdivi-1 groups were counteracted by fccp (Fig. 8I and J). Besides, we evaluated the relationship between mitochondrial fission and vascular function. Fission activator fccp partially counteracted the increase in Ve-cadherin and decrease in Icam and Vcam expressions engendered by the hydrogel (Fig. 8K and L). Together, these data demonstrate that the dual-loaded hydrogel protects microvascular function and promotes HUVECs migration and neovascularization by interfering with mitochondrial fission, reducing mtROS production, and protecting F-actin homeostasis, thereby accelerating the healing of chronic diabetic wounds (Fig. 8M).

3. Conclusions

We engineered a self-healing, tissue adhesive, antioxidant, provascular, dual-loaded hydrogel that can be used to promote chronic diabetic wound healing. The hydrogel exhibits a stable 3D structure with a highly interconnected porous network, which facilitates the mobility and release of bioactive substances and is well suited for the delivery of exosomes and metformin. We verified the ability of the hydrogel to

benefit diabetic wound healing, including maintaining microvessel integrity and barrier function, inhibiting inflammation, and promoting cell proliferation and angiogenesis. Furthermore, the dual-loaded hydrogel reduced mtROS and cellular ROS production and protected F-actin homeostasis in high-glucose environment by interfering with mitochondrial fission. This study revealed the potential therapeutic mechanism of exosome/metformin-loaded conductive hydrogel for treating chronic diabetic wounds.

4. Experimental section

4.1. Materials

4-Arm-PEG-Thiol was purchased from Xi'an Ruixi Biotechnology Co., Ltd. $AgNO_3$ was obtained from Sigma-Aldrich. Metformin hydrochloride was purchased from Beijing J&K Chemical Technology. Hydroxyl-modified MWCNTs with 10–20-nm diameter, 10–30-μm length, ≥100-S/cm conductivity, and ≥200-m^2/g special surface area were obtained from Nanjing XFNANO Materials Tech Co. All reagents were of analytical grade and used directly without further purification.

4.2. Preparation of the injectable, adhesive, self-healing exosome-hydrogels

The injectable, adhesive, self-healing exosome-hydrogels were prepared via Ag–S coordination between 4-Arm-PEG-Thiol and Ag^+. Briefly, exosomes extracted from human ADSCs were diluted to 100 μg/mL using PBS. 4-Arm-PEG-Thiol was dissolved in the exosome-containing PBS to prepare a solution with 13 wt% (w/v) concentration CNTs (4 mg/mL) were well dispersed in this solution owing to the hydrogen bonding between the hydroxyl groups on CNTs and thiol groups on 4-Arm-PEG-Thiol. Metformin hydrochloride (4 mg/mL) was further dissolved in the above mixture. Meanwhile, the stock solution of $AgNO_3$ (3 mg/mL) was prepared in PBS (pH = 7.4). Finally, PEG/Ag/CNT-M + E was prepared by mixing 500 μL 4-Arm-PEG-Thiol/exosome/CNTs/Met solution and 500 μL $AgNO_3$ stock solution. Moreover, based on the PEG/Ag/CNT-M + E hydrogel, the hydrogels prepared by removing different components were PEG/Ag (4-Arm-PEG-Thiol/$AgNO_3$), PEG/Ag/CNT (4-Arm-PEG-Thiol/$AgNO_3$/CNTs), PEG/Ag/CNT-M (4-Arm-PEG-Thiol/$AgNO_3$/CNTs/Met), and PEG/Ag/CNT-E(4-Arm-PEG-Thiol/$AgNO_3$/CNTs/exosome), respectively, where the components of each hydrogel have been provided in the brackets following the name. The preparation of the above hydrogels was the same as that of PEG/Ag/CNT-M + E hydrogel. The detailed composition of all the above hydrogels are shown in Table 1.

Table 1
Detailed compositions of the five hydrogels.

Sample	SH-4 arm PEG (mg/mL)	$AgNO_3$ (mg/mL)	CNTs (mg/mL)	Metformin (mg/mL)	Exosome (mg/mL)
PEG/Ag	65	1.5	/	/	/
PEG/Ag/CNT	65	1.5	2	/	/
PEG/Ag/CNT-M	65	1.5	2	1	/
PEG/Ag/CNT-E	65	1.5	2	/	0.1
PEG/Ag/CNT-M + E	65	1.5	2	1	0.1

4.3. Statistical analysis

All data were analyzed using SPSS 17.0 software and are presented as mean ± SD. Student's t-test was used for comparisons between two groups, and analysis of variance was used for multigroup comparisons. In all cases, if $p < 0.05$, there is a significant difference.

Notes

The authors declare no competing financial interest.

Ethics approval and consent to participate

All animal procedures were carried out in accordance with the principles of ARRIVE and approved by the Ethics Committee of Fourth Military Medical University.

CRediT authorship contribution statement

Yue Zhang: performed the experiments, and, analysized study data. **Meng Li:** performed the experiments, and, analysized study data. **Yunchuan Wang:** performed the experiments, and, analysized study data. **Fei Han:** provided study materials, reagents and materials. **Kuo Shen:** provided study materials, reagents and materials. **Liang Luo:** provided study materials, reagents and materials. **Yan Li:** provided study materials, reagents and materials. **Yanhui Jia:** provided study materials, reagents and materials. **Jian Zhang:** replicated the results. **Weixia Cai:** replicated the results. **Kejia Wang:** replicated the results. **Ming Zhao:** replicated the results. **Jing Wang:** provided laboratory samples and animals. **Xiaowen Gao:** provided laboratory samples and animals. **Chenyang Tian:** provided laboratory samples and animals, All authors read and approved the final manuscript. **Baolin Guo:** designed experiments, and, research methods. **Dahai Hu:** designed experiments, and, research methods.

Declaration of competing interest

All the authors declare no competing financial interest.

Acknowledgement

Yue Zhang, Meng Li and Yunchuan Wang contributed equally to this work. This work was supported by National Natural Science Foundation of China Youth Science Fund Project (No.82002039); National Natural Science Foundation of China (81530064); National Natural Science Foundation of China (81772071); National Natural Science Foundation of China (No.82172210).

Appendix A. Supplementary data

Supplementary data to this article can be found online at https://doi.org/10.1016/j.bioactmat.2023.01.020.

Abbreviations

ADSCs	adipose-derived stem cells
BG	blood glucose
BM	basement membrane
DMEM	Dulbecco's modified eagle medium
DPBS	Dulbecco's PBS
ECM	extracellular cellular matrix
H&E	hematoxylin and eosin
HUVECs	human umbilical vein endothelial cells
MTS	Materials Test System
MWCNT	multiwalled carbon nanotubes
PBS	phosphate-buffered saline
ROS	reactive oxygen species
TJ	tight junctions

References

[1] J.E. Shaw, R.A. Sicree, P.Z. Zimmet, Global estimates of the prevalence of diabetes for 2010 and 2030, Diabetes Res. Clin. Pract. 87 (1) (2010) 4–14.
[2] T. Hart, R. Milner, A. Cifu, Management of a diabetic foot, JAMA 318 (14) (2017) 1387–1388.
[3] Q. Bai, et al., Potential applications of nanomaterials and Technology for diabetic wound healing, Int. J. Nanomed. 15 (2020) 9717–9743.
[4] L. Deng, et al., The role of oxidative stress and antioxidants in diabetic wound healing, Oxid. Med. Cell. Longev. (2021), 8852759, 2021.
[5] J.L. Burgess, et al., Diabetic wound-healing science, Medicina (Kaunas) 57 (10) (2021).
[6] X. Qin, et al., Berberine protects glomerular podocytes via inhibiting drp1-mediated mitochondrial fission and dysfunction, Theranostics 9 (6) (2019) 1698–1713.
[7] Y. Zheng, A. Luo, X. Liu, The imbalance of mitochondrial fusion/fission drives high-glucose-induced vascular injury, Biomolecules 11 (12) (2021).
[8] H. Zhou, et al., Empagliflozin rescues diabetic myocardial microvascular injury via AMPK-mediated inhibition of mitochondrial fission, Redox Biol. 15 (2018) 335–346.
[9] S.M. Shenouda, et al., Altered mitochondrial dynamics contributes to endothelial dysfunction in diabetes mellitus, Circulation 124 (4) (2011) 444–453.
[10] H. Zhao, et al., Protective effect of trans-delta-viniferin against high glucose-induced oxidative stress in human umbilical vein endothelial cells through the SIRT1 pathway, Free Radic. Res. 50 (1) (2016) 68–83.
[11] S. Yang, et al., SIRT3 deficiency delays diabetic skin wound healing via oxidative stress and necroptosis enhancement, J. Cell Mol. Med. 24 (8) (2020) 4415–4427.
[12] S. Fernandez-Francos, et al., Mesenchymal stem cells as a cornerstone in a galaxy of intercellular signals: basis for a new era of medicine, Int. J. Mol. Sci. 22 (7) (2021).
[13] N. Naderi, et al., The regenerative role of adipose-derived stem cells (ADSC) in plastic and reconstructive surgery, Int. Wound J. 14 (1) (2017) 112–124.
[14] T.N. Dung, et al., Autologous adipose-derived stem cell (ADSC) transplantation in the management of chronic wounds, Ann Burns Fire Disasters 34 (4) (2021) 343–350.
[15] A. Chen, et al., Exosomes: biomarkers and therapeutic targets of diabetic vascular complications, Front. Endocrinol. 12 (2021), 720466.
[16] X. Li, et al., Exosomes from adipose-derived stem cells overexpressing Nrf2 accelerate cutaneous wound healing by promoting vascularization in a diabetic foot ulcer rat model, Exp. Mol. Med. 50 (4) (2018) 1–14.
[17] T. Wang, et al., MSC-derived exosomes protect against oxidative stress-induced skin injury via adaptive regulation of the NRF2 defense system, Biomaterials 257 (2020), 120264.
[18] X. Liu, et al., Exosomes secreted from human-induced pluripotent stem cell-derived mesenchymal stem cells prevent osteonecrosis of the femoral head by promoting angiogenesis, Int. J. Biol. Sci. 13 (2) (2017) 232–244.
[19] J. Lin, et al., Microenvironment-protected exosome-hydrogel for facilitating endometrial regeneration, fertility restoration, and live birth of offspring, Small 17 (11) (2021), e2007235.
[20] A. Chen, et al., Exosomes: biomarkers and therapeutic targets of diabetic vascular complications, Front. Endocrinol. 12 (2021), 720466.
[21] J. Lin, et al., Microenvironment-protected exosome-hydrogel for facilitating endometrial regeneration, fertility restoration, and live birth of offspring, Small 17 (11) (2021), e2007235.
[22] C. Niu, et al., Metformin alleviates hyperglycemia-induced endothelial impairment by downregulating autophagy via the Hedgehog pathway, Autophagy 15 (5) (2019) 843–870.
[23] Y. Hattori, et al., Metformin inhibits cytokine-induced nuclear factor kappaB activation via AMP-activated protein kinase activation in vascular endothelial cells, Hypertension 47 (6) (2006) 1183–1188.
[24] C.J. Bailey, Metformin: historical overview, Diabetologia 60 (9) (2017) 1566–1576.
[25] Corrigendum to: anti-aging pharmacology in cutaneous wound healing: effects of metformin, resveratrol, and rapamycin by local application, Aging Cell 21 (2) (2022), e13561.
[26] Y. Liang, et al., pH/glucose dual responsive metformin release hydrogel dressings with adhesion and self-healing via dual-dynamic bonding for athletic diabetic foot wound healing, ACS Nano 16 (2) (2022) 3194–3207.
[27] L. Zhao, et al., pH and glucose dual-responsive injectable hydrogels with insulin and fibroblasts as bioactive dressings for diabetic wound healing, ACS Appl. Mater. Interfaces 9 (43) (2017) 37563–37574.
[28] Y. Xiong, et al., All-in-One: multifunctional hydrogel accelerates oxidative diabetic wound healing through timed-release of exosome and fibroblast growth factor, Small 18 (1) (2022), e2104229.
[29] Y. Liang, J. He, B. Guo, Functional hydrogels as wound dressing to enhance wound healing, ACS Nano 15 (8) (2021) 12687–12722.
[30] K.C. Broussard, J.G. Powers, Wound dressings: selecting the most appropriate type, Am. J. Clin. Dermatol. 14 (6) (2013) 449–459.
[31] T.V.R. Op, et al., Design considerations for hydrogel wound dressings: strategic and molecular advances, Tissue Eng. B Rev. 26 (3) (2020) 230–248.
[32] A. Oryan, et al., Healing potential of injectable Aloe vera hydrogel loaded by adipose-derived stem cell in skin tissue-engineering in a rat burn wound model, Cell Tissue Res. 377 (2) (2019) 215–227.
[33] S. Chen, et al., Mesenchymal stem cell-laden anti-inflammatory hydrogel enhances diabetic wound healing, Sci. Rep. 5 (2015), 18104.
[34] M.M. Martino, et al., Heparin-binding domain of fibrin(ogen) binds growth factors and promotes tissue repair when incorporated within a synthetic matrix, Proc. Natl. Acad. Sci. U. S. A. 110 (12) (2013) 4563–4568.
[35] A. Zhang, et al., Research status of self-healing hydrogel for wound management: a review, Int. J. Biol. Macromol. 164 (2020) 2108–2123.
[36] F. Sun, et al., An injectable and instant self-healing medical adhesive for wound sealing, ACS Appl. Mater. Interfaces 12 (8) (2020) 9132–9140.
[37] B. Guo, et al., Degradable conductive self-healing hydrogels based on dextran-graft-tetraaniline and N-carboxyethyl chitosan as injectable carriers for myoblast cell therapy and muscle regeneration, Acta Biomater. 84 (2019) 180–193.
[38] M.P. Nikolova, M.S. Chavali, Recent advances in biomaterials for 3D scaffolds: a review, Bioact. Mater. 4 (2019) 271–292.
[39] X. Zhao, et al., Antibacterial anti-oxidant electroactive injectable hydrogel as self-healing wound dressing with hemostasis and adhesiveness for cutaneous wound healing, Biomaterials 122 (2017) 34–47.
[40] M. Nikkhah, J. Rivnay, Conductive and electroactive biomaterials and bioelectronics, Acta Biomater. 139 (2022) 1–3.
[41] L. Mao, et al., Biodegradable and electroactive regenerated bacterial cellulose/MXene (Ti3 C2 tx) composite hydrogel as wound dressing for accelerating skin wound healing under electrical stimulation, Adv Healthc Mater 9 (19) (2020), e2000872.
[42] E.L. Hopley, et al., Carbon nanotubes leading the way forward in new generation 3D tissue engineering, Biotechnol. Adv. 32 (5) (2014) 1000–1014.
[43] A. Masotti, et al., Regulation of angiogenesis through the efficient delivery of microRNAs into endothelial cells using polyamine-coated carbon nanotubes, Nanomedicine 12 (6) (2016) 1511–1522.
[44] J. Saravana, B. Arunpandian, I.A. Fauzi, et al., Fabrication and hemocompatibility assessment of novel polyurethane-based bio-nanofibrous dressing loaded with honey and Carica papaya extract for the management of burn injuries[J], Int. J. Nanomed. 11 (2016) 4339–4355.
[45] C. Hou, et al., Investigation on clotting and hemolysis characteristics of heparin-immobilized polyether sulfones biomembrane, J. Biomed. Mater. Res. 85 (3) (2008) 847–852.
[46] ISO E, 10993–4. Biological Evaluation of Medical Devices-Part 4: Selection of Tests for Interactions with, blood, 2006.
[47] ASTM. F, 756–00: Standard Practice for Assessment of Hemolytic Properties of Materials, Annual Book of ASTM Standards; American Society of Testing and Materials, West Conshohocken, PA, 2000.
[48] Y. Liang, X. Zhao, T. Hu, et al., Adhesive hemostatic conducting injectable composite hydrogels with sustained drug release and photothermal antibacterial activity to promote full-thickness skin regeneration during wound healing[J], Small 15 (12) (2019).
[49] R.O. Forsythe, J. Brownrigg, R.J. Hinchliffe, Peripheral arterial disease and revascularization of the diabetic foot, Diabetes Obes. Metabol. 17 (5) (2015) 435–444.
[50] R.O. Forsythe, J. Brownrigg, R.J. Hinchliffe, Peripheral arterial disease and revascularization of the diabetic foot, Diabetes Obes. Metabol. 17 (5) (2015) 435–444.
[51] Y. Shi, P.M. Vanhoutte, Macro- and microvascular endothelial dysfunction in diabetes, J. Diabetes 9 (5) (2017) 434–449.
[52] J.L. Burgess, et al., Diabetic wound-healing science, Medicina (Kaunas) 57 (10) (2021).
[53] S. Sangiorgi, et al., The cutaneous microvascular architecture of human diabetic toe studied by corrosion casting and scanning electron microscopy analysis, Anat. Rec. 293 (10) (2010) 1639–1645.
[54] E. Choke, et al., Treatment of lower limb ischaemia in patients with diabetes, Diabetes Metab Res Rev 36 (1) (2020), e3262.
[55] Z. Ma, et al., Multilayer injectable hydrogel system sequentially delivers bioactive substances for each wound healing stage, ACS Appl. Mater. Interfaces 12 (26) (2020) 29787–29806.
[56] D.G. Phinney, M.F. Pittenger, Concise review: MSC-derived exosomes for cell-free therapy, Stem Cell. 35 (4) (2017) 851–858.
[57] M.A. Brennan, P. Layrolle, D.J. Mooney, Biomaterials functionalized with MSC secreted extracellular vesicles and soluble factors for tissue regeneration, Adv. Funct. Mater. 30 (37) (2020).
[58] M. Giannotta, M. Trani, E. Dejana, VE-cadherin and endothelial adherens junctions: active guardians of vascular integrity, Dev. Cell 26 (5) (2013) 441–454.
[59] D. Vestweber, VE-cadherin: the major endothelial adhesion molecule controlling cellular junctions and blood vessel formation, Arterioscler. Thromb. Vasc. Biol. 28 (2) (2008) 223–232.
[60] G.V. Ganesh, K.M. Ramkumar, Macrophage mediation in normal and diabetic wound healing responses, Inflamm. Res. 69 (4) (2020) 347–363.
[61] M. Kloc, et al., Macrophage functions in wound healing, J Tissue Eng Regen Med 13 (1) (2019) 99–109.
[62] A.E. Louiselle, et al., Macrophage polarization and diabetic wound healing, Transl. Res. 236 (2021) 109–116.
[63] M. Li, et al., Macrophage related chronic inflammation in non-healing wounds, Front. Immunol. 12 (2021), 681710.
[64] S.A. Jones, B.J. Jenkins, Recent insights into targeting the IL-6 cytokine family in inflammatory diseases and cancer, Nat. Rev. Immunol. 18 (12) (2018) 773–789.
[65] P.A. Nigrovic, P.Y. Lee, H.M. Hoffman, Monogenic autoinflammatory disorders: conceptual overview, phenotype, and clinical approach, J. Allergy Clin. Immunol. 146 (5) (2020) 925–937.
[66] R.O. Forsythe, J. Brownrigg, R.J. Hinchliffe, Peripheral arterial disease and revascularization of the diabetic foot, Diabetes Obes. Metabol. 17 (5) (2015) 435–444.

[67] M. Brownlee, Biochemistry and molecular cell biology of diabetic complications, Nature 414 (6865) (2001) 813–820.
[68] X. Li, et al., SIRT1 activation promotes angiogenesis in diabetic wounds by protecting endothelial cells against oxidative stress, Arch. Biochem. Biophys. 661 (2019) 117–124.
[69] J.S. Johansen, et al., Oxidative stress and the use of antioxidants in diabetes: linking basic science to clinical practice, Cardiovasc. Diabetol. 4 (2005) 5.
[70] S. Yang, et al., SIRT3 deficiency delays diabetic skin wound healing via oxidative stress and necroptosis enhancement, J. Cell Mol. Med. 24 (8) (2020) 4415–4427.
[71] A.M. El, J. Angulo, L. Rodriguez-Manas, Oxidative stress and vascular inflammation in aging, Free Radic. Biol. Med. 65 (2013) 380–401.
[72] M. Mittal, et al., Reactive oxygen species in inflammation and tissue injury, Antioxidants Redox Signal. 20 (7) (2014) 1126–1167.
[73] F. Paneni, et al., Diabetes and vascular disease: pathophysiology, clinical consequences, and medical therapy: part I, Eur. Heart J. 34 (31) (2013) 2436–2443.
[74] M.E. Widlansky, R.B. Hill, Mitochondrial regulation of diabetic vascular disease: an emerging opportunity, Transl. Res. 202 (2018) 83–98.
[75] S. Rovira-Llopis, et al., Mitochondrial dynamics in type 2 diabetes: pathophysiological implications, Redox Biol. 11 (2017) 637–645.
[76] S. Belhadj, et al., Beneficial effect of jojoba seed extracts on hyperglycemia-induced oxidative stress in RINm5f beta cells, Nutrients 10 (3) (2018).
[77] M.E. Widlansky, R.B. Hill, Mitochondrial regulation of diabetic vascular disease: an emerging opportunity, Transl. Res. 202 (2018) 83–98.
[78] I.N. Zelko, T.J. Mariani, R.J. Folz, Superoxide dismutase multigene family: a comparison of the CuZn-SOD (SOD1), Mn-SOD (SOD2), and EC-SOD (SOD3) gene structures, evolution, and expression, Free Radic. Biol. Med. 33 (3) (2002) 337–349.
[79] T. Nishikawa, et al., Normalizing mitochondrial superoxide production blocks three pathways of hyperglycaemic damage, Nature 404 (6779) (2000) 787–790.
[80] Y. Zheng, A. Luo, X. Liu, The imbalance of mitochondrial fusion/fission drives high-glucose-induced vascular injury, Biomolecules 11 (12) (2021).
[81] S.M. Shenouda, et al., Altered mitochondrial dynamics contributes to endothelial dysfunction in diabetes mellitus, Circulation 124 (4) (2011) 444–453.
[82] A. Li, et al., Metformin and resveratrol inhibit Drp1-mediated mitochondrial fission and prevent ER stress-associated NLRP3 inflammasome activation in the adipose tissue of diabetic mice, Mol. Cell. Endocrinol. 434 (2016) 36–47.
[83] H. Zhou, et al., Empagliflozin rescues diabetic myocardial microvascular injury via AMPK-mediated inhibition of mitochondrial fission, Redox Biol. 15 (2018) 335–346.
[84] C. Shi, et al., Yap promotes hepatocellular carcinoma metastasis and mobilization via governing cofilin/F-actin/lamellipodium axis by regulation of JNK/Bnip3/SERCA/CaMKII pathways, Redox Biol. 14 (2018) 59–71.
[85] Y. Liu, et al., Endothelial cytoskeletal elements are critical for flow-mediated dilation in human coronary arterioles, Med. Biol. Eng. Comput. 46 (5) (2008) 469–478.
[86] A.L. Hatch, et al., Actin filaments as dynamic reservoirs for Drp1 recruitment, Mol. Biol. Cell 27 (20) (2016) 3109–3121.
[87] S. Li, et al., Transient assembly of F-actin on the outer mitochondrial membrane contributes to mitochondrial fission, J. Cell Biol. 208 (1) (2015) 109–123.
[88] S. Preau, et al., Endotoxemia engages the RhoA kinase pathway to impair cardiac function by altering cytoskeleton, mitochondrial fission, and autophagy, Antioxidants Redox Signal. 24 (10) (2016) 529–542.
[89] J. Prudent, H.M. McBride, Mitochondrial dynamics: ER actin tightens the Drp1 noose, Curr. Biol. 26 (5) (2016) R207–R209.